doi:10.1016/j.jmb.2005.04.071 J. Mol. Biol. (2005) 350, 599–608

JMB

Available online at www.sciencedirect.com

SCIENCE DIRECT®

ELSEVIER

Structural Basis for the Thermostability of Ferredoxin from the Cyanobacterium *Mastigocladus laminosus*

Alexander Fish[1,2], Tsafi Danieli[2], Itzhak Ohad[3], Rachel Nechushtai[1,2] and Oded Livnah[2,3]*

[1]*The Department of Plant Sciences, The Institute of Life Sciences, The Hebrew University of Jerusalem, Givat Ram, Jerusalem 91904, Israel*

[2]*The Wolfson Centre for Applied Structural Biology The Institute of Life Sciences The Hebrew University of Jerusalem, Givat Ram, Jerusalem 91904, Israel*

[3]*The Department of Biological Chemistry, The Institute of Life Sciences, The Hebrew University of Jerusalem, Givat Ram, Jerusalem 91904, Israel*

**Corresponding author*

Plant-type ferredoxins (Fds) carry a single [2Fe-2S] cluster and serve as electron acceptors of photosystem I (PSI). The ferredoxin from the thermophilic cyanobacterium *Mastigocladus laminosus* displays optimal activity at 65 °C. In order to reveal the molecular factors that confer thermostability, the crystal structure of *M. laminosus* Fd (mFd) was determined to 1.25 Å resolution and subsequently analyzed in comparison with four similar plant-type mesophilic ferredoxins. The topologies of the plant-type ferredoxins are similar, yet two structural determinants were identified that may account for differences in thermostability, a salt bridge network in the C-terminal region, and the flexible L1,2 loop that increases hydrophobic accessible surface area. These conclusions were verified by three mutations, i.e. substitution of L1,2 into a rigid β-turn (ΔL1,2) and two point mutations (E90S and E96S) that disrupt the salt bridge network at the C-terminal region. All three mutants have shown reduced electron transfer (ET) capabilities and [2Fe-2S] stability at high temperatures in comparison to the wild-type mFd. The results have also provided new insights into the involvement of the L1,2 loop in the Fd interactions with its electron donor, the PSI complex.

Keywords: photosystem I; photosynthesis; thermostability; X-ray structure; ferredoxin

Introduction

Ferredoxins (Fds) are soluble iron-sulfur proteins, found in bacteria, plants, and mammalian cells, which are involved in numerous electron transfer reactions. Fds are characterized and classified by their prosthetic groups, i.e. the presence of one or two iron-sulfur clusters of the types [4Fe-4S], [3Fe-4S] or [2Fe-2S].[1–3] Fds from plants, algae, and photosynthetic bacteria, denoted as plant-type ferredoxins, have a single [2Fe-2S] cluster in which each iron atom is coordinated by four sulfur ligands including two inorganic sulfur atoms, which bridge the two iron (Fe^{3+}) ions, and two sulfur atoms from the cysteine side-chains of the Fd. The four sulfur atoms are organized in an approximately tetrahedral arrangement around each iron atom and the three-dimensional structure in the vicinity of the iron-sulfur cluster is highly conserved in many plant-type Fds.[4,5] The oxidation–reduction midpoint potential (E_m) values of these Fds are typically around −0.42 eV,[6] making the reduced form of these Fds one of the strongest soluble reducing agents known in nature. It serves as the electron donor in several essential reactions such as $NADP^+$ reduction, where FNR is the active enzyme, carbon assimilation, nitrite reduction for nitrogen assimilation, sulfite reduction, glutamate synthesis and thioredoxin reduction for metabolism regulation.[4] The reduction of plant-type Fd is directly accomplished by the photosystem I reaction center during oxygenic photosynthesis.[7]

Fd isolated from the thermophilic cyanobacterium *Mastigocladus laminosus* (mFd), has been shown to display thermostable properties, with maximal activity at 65 °C.[8] Although the thermostability of mFd was discovered more than 20 years ago,[8]

Present address: O. Livnah, The Department of Biological Chemistry, The Silberman Institute of Life Sciences, The Wolfson Centre for Applied Structural Biology, The Hebrew University of Jerusalem, Safra Campus, Givat Ram, Jerusalem 91904, Israel.

Abbreviations used: mFd, *Mastigocladus laminosus* ferredoxin; PSI, photosystem I; ET, electron transfer; wt, wild-type; ASA, accessible surface area.

E-mail address of the corresponding author: oded.livnah@huji.ac.il

its determinants remain unsolved. The factors that determine thermostability in proteins are under considerable investigation.[9–13] These studies have indicated that features that strongly influence the thermostability of a protein[12,14,15] include better or tighter atom packing, the ratio between polar surface and buried hydrophobic surface areas, and salt bridge formation. Further studies indicate that in many instances a combination of selected factors render a protein thermostable.[16]

The primary structures of Fds are well characterized in more than 70 plants, algae and cyanobacteria. The three-dimensional crystal structures of 20 plant-type Fds have been determined to relatively high resolution and are available in the RCSB Protein Data Bank.[17] These crystal structures are derived from ten different mesophilic organisms (having an ideal growth temperature of 20 °C to 45 °C). In addition, two Fd structures from the thermophilic cyanobacterium *Synechococcus elongatus*[18,19] have been determined using nuclear magnetic resonance (NMR) spectroscopy techniques. To date, however, analysis of the thermostability determining factors in these Fd structures is still inconclusive.

Here, we have identified factors that affect the thermostability of mFd by solving its crystal structure to a resolution of 1.25 Å. A detailed structural comparison of the primary and tertiary structures of the thermophilic mFd with four highly related mesophilic Fd proteins suggested two molecular factors which cause thermostability in mFd: a salt bridge network at the C terminus of the protein, and the flexibility of the loop connecting β1 and β2 strands (L1,2). To verify these findings, three site-directed mutations were designed and their ability to accept electrons from PSI was compared to that of the wild-type (wt) mFd, as well as the thermal stability of their [2Fe-2S] clusters.

Results

Structure determination of mFd

The structure of mFd was determined by molecular replacement methods using the monomer structure of the D68K mutant of *Anabaena* sp. PCC 7120 (PDB code 1J7C)[20] without the solvent molecules as the search model. The best molecular replacement solution resulted in an *R*-factor of 35.2% and a correlation coefficient of 77.8% at the resolution range of 10.0 Å–4.0 Å with two molecules in the asymmetric unit. The structure was initially refined using the rigid body procedure in CNS,[21] and was then further refined using SHELX-97 at the resolution range of 20.0 Å–1.25 Å (Table 1).[22] The model was built and fitted into the $F_{obs}-F_{calc}$ and $2F_{obs}-F_{calc}$ electron density maps (Figure 1) using the graphics program O.[23] The model was refined and fitted into the electron density maps for 12 iterative cycles at the resolution range of 20.0 Å–1.25 Å, to the final crystallographic *R*-value of 19.9% and R_{free} of 24.7% (Table 1). Residues Asn15, Glu19, Asp28, Ser40, Lys52, Ile54, Ser61, Ser62, Ile71, Val76, Cys87 for molecule A and Lys4, Lys16, Ser40, Ile54, Glu72, Val76, Cys87 for molecule B have multiple side-chain conformations. The final model of mFd consists of residues 1–9, 14–98 for monomer A, residues 1–97 for monomer B, as well as eight cluster atoms and 244 solvent molecules. The coordinates of mFd (PDB code 1RFK) are available from the RCSB Protein Data Bank.[17]

Table 1. Data collection and refinement statistics of *M. laminosus* ferredoxin

Space group	$P2_12_12_1$
Resolution (Å)	20–1.25
Unique reflections	44,557
Redundancy	6.5
$R_{sym}(I)$[a]	6.5(24.7)[b]
Completeness (%)	98.0(96.0)
I/σ	18.9(4.3)
Number of protein atoms	1482
Number of ligand atoms	8
Number of solvent atoms	244
R-factor (all *F*; $F>4\sigma$)	0.199; 0.193
R_{free} (all *F*; $F>4\sigma$)[c]	0.247; 0.241
Average *B* factor (Å^2)	
Protein	14.3
Cluster	9.5
Solvent	28.3
RMSD from ideality	
Bond lengths (Å)	0.014
Bond angles (deg.)	2.2
Ramachandran plot[d] number of non-glycine and non-proline residues (%)	
Favored	(149) 88.2
Allowed	(19) 11.2
Generously allowed	(1) 0.6
Disallowed	(0) 0.0

[a] $R_{sym}(I) = \Sigma|I - \langle I\rangle|/\Sigma I$.
[b] Outer shell resolution range (1.27 Å–1.25 Å)
[c] The test set is 5% of data.
[d] The structure quality was evaluated using PROCHECK 4.[52]

The structure of mFd is characterized by a central core formed by five β-strands β1–β3, β5 and β7 and an α-helix (α1) positioned above the β-sheet (Figure 2) to form a "β-grasp" motif.[24,25] The [2Fe-2S]

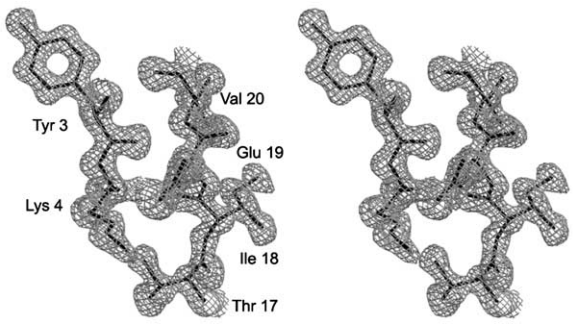

Figure 1. A representative $2F_{obs}-F_{calc}$ electron density map. The $2F_{obs}-F_{calc}$ map was calculated at a resolution range of 20 Å–1.25 Å and contoured at 1.4σ cutoff of the refined mFd structure. The section consists of residues 3–4 and 17–20 from molecule A of *M. laminosus* ferredoxin. The Figure was drawn using BOBSCRIPT.[48]

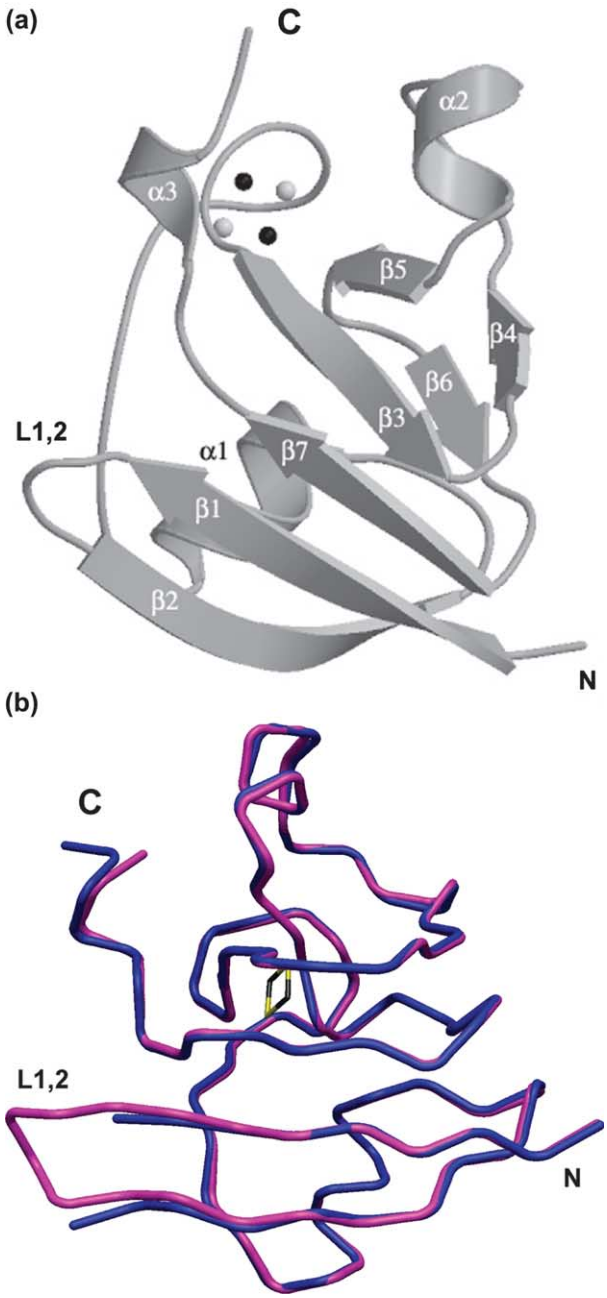

Figure 2. The structure of *M. laminosus* ferredoxin. (a) MOLSCRIPT[49] ribbon diagram of the molecule B from *M. laminosus* ferredoxin. The secondary structure elements as well as the termini and the L1,2 loop region, are labeled. The [2Fe-2S] cluster is positioned in a solvent-exposed pocket where the Fe and S atoms are colored in black and gray, respectively. The structure is characterized by a central core formed by a β-sheet composed of strands β1–β3, β5 andβ7 and an α-helix (α1) positioned above to form a β-grasp motif. (b) Superposition of the A and B molecules of *M. laminosus* ferredoxin. Tube representations of molecule A in blue and molecule B in magenta are presented. The [2Fe-2S] cluster of molecule A is shown in stick representation, where the Fe and S atoms are colored black and yellow, respectively. The largest differences between the two molecules are located in the L1,2 loop region where molecule A has no apparent electron density for residues 10–14, which are thus not built into the model. The model was constructed using the graphics program MIDAS.[50]

cluster is located in a solvent-exposed pocket formed by the loop connecting helix α1 with strand β3. This loop contains three of the four cysteine residues (Cys41, Cys46 and Cys49) which coordinate the two iron ions. The forth cysteine residue (Cys79) is contributed from the loop connecting strands β5 and β6. There are two major conformational differences between the two mFd molecules (A and B) in the asymmetric unit. The first is located in the C-terminal segment (residues 94–98) and the second in the loop region connecting β1 and β2, residues 10–14 (L1,2), which is not traced in molecule A (Figure 2(a)) due to the lack of interpretable electron density map. The differences between the two mFd molecules in the L1,2 region may be attributed to crystal packing considerations. The L1,2 loop region in molecule A has no noticeable symmetry-related molecules in its vicinity to form any stabilizing interactions. In molecule B, however, loop L1,2 forms H-bond interactions due to crystal packing. These crystal contacts sustain conformational stability in the L1,2 loop region of molecule B, yet the flexibility of L1,2 in molecule A may reflect its flexibility in solution. In this context, the average temperature factors of the L1,2 region in molecule B is higher relative to the entire monomer (22.8 $Å^2$ and 15.6 $Å^2$, respectively). Superposition of the two molecules (Figure 2(b)) results in a root-mean-square deviation (RMSD) of 0.46 Å (for 94 C^α pairs) and 0.298 Å (for 88 C^α pairs, removing residues 10–14 and 94–98).

Structural comparison of mFd with selected mesophilic Fds

The structure of mFd was compared to four selected plant-type Fd molecules based on high sequence identity. Three Fd structures originated from mesophilic cyanobacteria *Anabaena* sp. PCC 7119 (aFd) (PDB code 1QT9),[26] *Spirulina platensis* (pFd) [PDB code 4FXC][24] and *Synechocystis* sp. PCC 6803 (sFd) (PDB code 1OFF)[27] (Figure 3(a) and Table 2). Fd from the higher plant *Spinacia oleracea* (oFd) (PDB code 1A70)[28] was also elected for evaluation based on its relatively high sequence identity (68%) with mFd (Figure 3(a) and Table 2). The overall folding pattern of mFd is highly similar to all available plant-type Fd structures. Structural superposition of mFd with the four selected Fd structures indicated significant differences in the conformation of the L1,2 loop (Figure 3(b)). Sequence alignment also revealed some differences in the L1,2 loop region, indicating that oFd and sFd are two residues shorter than the other Fd molecules. The shorter L1,2 loop forms a β-turn in the molecules of oFd and sFd (Figure 3(a)) rather than the hairpin loop present in mFd, aFd, and pFd. The three disordered residues (Glu10, Ala11 and Glu12) in the mFd molecule A illustrate the flexibility of the L1,2 region. Moreover, the different conformations of the L1,2 region in mFd (molecule B), aFd and pFd are restrained by non-functional

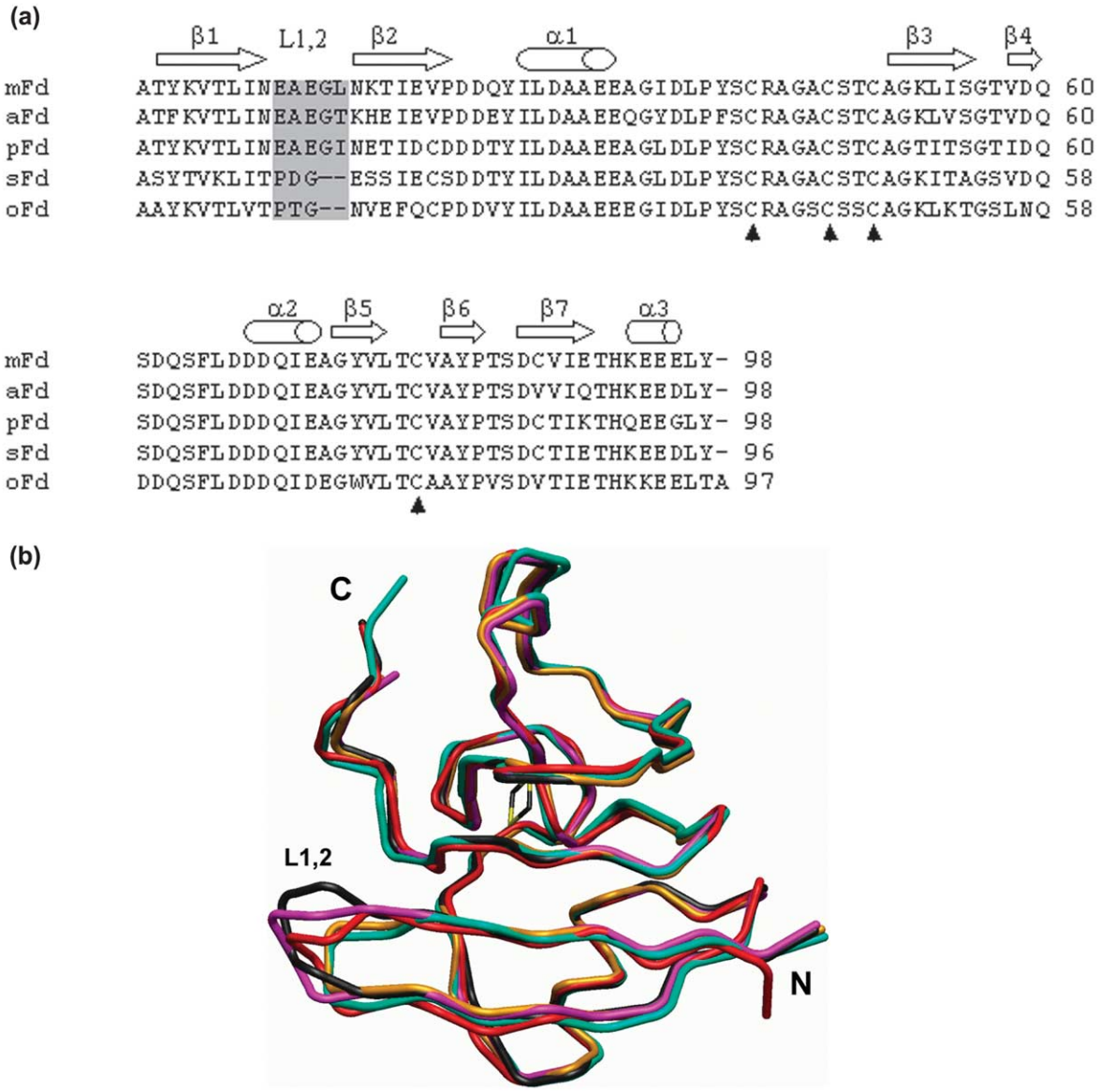

Figure 3. A structural comparison of *M. laminosus* ferredoxin to four mesophilic ferredoxin structures. (a) Sequence alignment of the five ferredoxin molecules was performed using CLUSTAL W.[51] The L1,2 loop region is highlighted in gray and the secondary structure motifs are shown in arrows for β-strands and cylinders for α-helices. The four cysteine residues that coordinate the Fe atoms in the [2Fe-2S] cluster are indicated with arrowheads. (b) Three-dimensional structural superposition of ferredoxins from *M. laminosus* ferredoxin–(mFd; magenta), *Anabaena* sp. PCC 7119 (black), *Spirulina platensis* (red), *Synechocystis* sp. PCC 6803 (gold), and *Spinacia oleracea* (cyan) molecules indicating the identical fold of the molecules. The [2Fe-2S] cluster of mFd is shown (stick representation). The L1,2 loop region is labeled and indicates the flexibility of the region in mFd, aFd and pFd. In sFd and oFd, the loop is two residues shorter, thus forming a β-turn. The model was constructed using the graphics program MIDAS.[50]

crystal contacts (for aFd and pFd the average *B* value of the L1,2 is similar to that of the entire molecules). Taken together, these observations indicate that the L1,2 loop regions in the three latter ferredoxins are most likely flexible in solution.

Analysis of molecular factors conferring thermal stability to mFd

Based on the structurally derived data, the factors known to affect thermostability in proteins[12,14,15] were analyzed for mFd, in comparison to the four selected mesophilic Fds (Table 3). There are no significant differences in the number of H-bond interactions among the five Fds analyzed. However, the numbers and volumes of internal cavities differ. For instance, the volume of the oFd cavity is much smaller than that of the other Fd molecules (Table 3). Nevertheless, the other parameters that indicate packing quality, such as packing density and surface-to-volume ratio, are similar for all Fd proteins analyzed. Although there is no significant difference in hydrophobic and hydrophilic accessible surface areas (ASA), the ratio of hydrophobic

Table 2. Structural comparison between *M. laminosus* Fd and the selected Fds

Molecule[a]	Resolution (Å)	Number of residues	Sequence identity (%)	RMSD[b]
aFd	1.3	98	86	0.34
pFd	2.5	98	84	0.49
sFd	1.8	96	78	0.41
oFd	1.7	97	68	0.50

[a] The comparison was made by superposing the known crystal structures of the following ferredoxins onto the molecule B of *M. laminosus* ferredoxin: *Anabaena* sp. PCC 7119 ferredoxin–(aFd),[26] *Spirulina platensis* ferredoxin–(pFd),[24] *Synechocystis* sp. PCC 6803 ferredoxin–(sFd)[27] and *S. oleracea* ferredoxin–(oFd).[28]
[b] Root-mean-square deviation (RMSD) from the superposition of C^{α} atoms homologous to residues 2–9 and 15–93 of *M. laminosus* Fd. The structure superposition was performed with the program O.[23]

to total ASA is slightly higher for mFd and aFd in comparison to other Fds. Analysis of salt bridge interactions among the different Fds resulted in five possible salt bridges in mFd as compared to three, two and four in the cyanobacterial aFd, pFd and sFd, respectively (Tables 3 and 4). The higher plant mesophilic oFd, however, contains six salt bridge interactions. Among all Fds analyzed, only a single salt bridge interaction between Arg42 and Glu31 was found conserved (Table 4).

In addition, there are salt bridge networks in mFd, sFd, and oFd as indicated in Figure 4. In mFd, Lys93 forms a two-salt bridge network with Glu90 and Glu96 (Figure 4, center). In sFd, Glu89 forms a salt bridge network with Lys51 and Lys92 (Figure 4, right). oFd contains a more intricate salt bridge network, which involves Glu88 and Lys91 (Figure 4, left). In aFd, however, Lys93 forms only a single salt bridge interaction with Glu10, and in pFd there are no salt bridge interactions in the C-terminal region (Table 4).

Analysis of the thermal stability of the [2Fe-2S] cluster and the ET activity of mFd wt and mutants

Based on our structural analysis, we elected to mutate mFd in order to verify whether our assumptions of the molecular factors that confer thermostability to mFd are correct. We focused on the L1,2 loop and the salt bridge network in the C-terminal region of mFd that displayed differences between thermostable mFd and the four mesophilic Fds. In the first mutant, ΔL1,2, the flexible L1,2 loop in mFd (residues 10–14) was replaced with the rigid β-turn of spinach Fd (residues 10–12). The other two point mutations, E90S and E96S, were designed to disrupt the salt bridge network at the C terminus of mFd.

The absorption values for wt mFd and the three designed mutants were measured at 280 nm and 423 nm, at increasing temperatures. The three mutants display a decrease in the 423 nm absorption at a lower temperature in comparison to the wt mFd (Figure 5), indicating a dissociation of the [2Fe-2S] cluster from the protein. A ∼10 deg. C decrease in [2Fe-2S] stability is seen in the two point mutations, E90S and E96S, in which fewer salt bridge interactions occur. The ΔL1,2 substitution of the L1,2 loop by a β-turn has a relatively smaller effect (∼5 deg. C) on [2Fe-2S] thermal stability (Figure 5). A temperature-dependent CD analysis of

Table 3. Structural statistics

	Protein				
Characteristics[a]	mFd[b]	aFd	pFd	sFd	oFd
Total number of H-bonds[c]	84	83	57	80	83
Number of MM H-bonds	52	52	42	48	51
Number of MS H-bonds	18	18	8	17	18
Number of SS H-bonds	14	13	7	15	14
Number of cavities[d]	1	1	3	3	1
Volume of cavities ($Å^3$)	71	73	107	84	17
Packing density[e]	0.46	0.46	0.48	0.48	0.47
Surface-to-volume ratio	0.36	0.36	0.36	0.37	0.37
Total ASA ($Å^2$)	5127	5115	5150	4816	5149
Charged ASA ($Å^2$)	1435	1507	1507	1410	1459
Polar ASA ($Å^2$)	1705	1579	1790	1698	1789
Hydrophobic ASA ($Å^2$)	1987	2029	1853	1708	1901
Hydrophobic ASA/total ASA (%)	39	40	36	35	37
Salt bridges[f]	5	3	2	4	6

[a] In all calculations, water molecules and hetero-atoms were excluded from the coordinate files.
[b] Data shown for molecule B of *M. laminosus* ferredoxin (mFd), *Anabaena* sp. PCC 7119 ferredoxin–(aFd),[26] *S. platensis* ferredoxin–(pFd),[24] *Synechocystis* sp. PCC 6803 ferredoxin–(sFd)[27] and *S. oleracea* ferredoxin–(oFd).[28]
[c] Number of hydrogen bonds were calculated using the HBPlus routine[53] with default parameters for distances and angles. The hydrogen bonds were divided into three classes: main-chain–main-chain (MM H-bonds), main-chain–side-chain (MS H-bonds), and side-chain–side-chain (SS H-bonds).
[d] The program GRASP (version 1.3) was used to provide cavity information and to calculate total and hydrophobic accessible surface areas (ASA).[54] The probe radius used was 1.4 Å and the surface resolution parameter was three points/Å. The charged/polar/hydrophobic ASAs were calculated based on individual chemical groups.
[e] Ratio of the van der Waals volume to volume enclosed by molecular surface.
[f] A salt bridge was inferred when Asp or Glu side-chain carbonyl oxygen atoms were found to be within 4.0 Å from the nitrogen atoms of Arg, Lys, or His side-chains.[16,55] A group of residues was defined as a salt bridge network if salt bridges connected them.

Table 4. Salt bridge interactions in the selected ferredoxin molecules

mFd		aFd		pFd		sFd		oFd	
R pair	dis[a]	R pair	dis	R pair	dis	R pair	dis	R pair	dis
Lys4–Glu19	3.52	Arg42–Asp28	2.82	Lys4–Asp19	3.98	Lys7–Glu14	3.15	Lys4–Glu15	3.14
Arg42–Asp28	2.97	Arg42–Glu31	2.80	Arg42–Glu31	3.03	Arg41–Glu30	2.83	Arg40–Asp26	3.27
			2.84		3.14		2.86		
Arg42–Glu31	2.81	Lys93–Glu10	2.86			Lys51–Glu89	2.92	Arg40–Glu29	2.74
	2.86								2.81
Lys93–Glu90	3.68					Lys92–Glu89	3.66	Lys52–Glu88	3.25
									3.47
Lys93–Glu96	2.73							Lys91–Glu88	3.07
	3.53								
								Lys91–Glu94	3.44
									3.49

The salt bridge interactions were analyzed based on the criteria described for Table 3. Data are shown for molecule B of *M. laminosus* ferredoxin (mFd), *Anabaena* sp. PCC 7119 ferredoxin–(aFd),[26] *S. platensis* ferredoxin–(pFd),[24] *Synechocystis* sp. PCC 6803 ferredoxin–(sFd)[27] and *S. oleracea* ferredoxin–(oFd).[28]

[a] Distance between interacting atoms (Å). Two values indicate the possibility of forming two salt bridge interactions (Figure 4).

the wt and two mutant Fds is in accord with the cluster stability assay (data not shown).

In addition, the ET from *M. laminosus* PSI to wt and the three mFd mutants was assayed and analyzed. The initial light-induced oxidation rate of *M. laminosus* PSI primary donor, P_{700}, by the wt and different mFd mutants was monitored using the PAM-101 system[29] at two temperatures of 23 °C and 55 °C (Table 5). The PSI photo-oxidation rate without mFd as an electron acceptor was used as a reference. At a temperature of 23 °C the wt and all three mutants did not show any significant differences in PSI oxidation. At the higher temperature of 55 °C, the ΔL1,2 mutant showed an extremely low ET capability, indicating that the mutant was unable to photo-oxidize PSI in light, whereas the E90S and E96S mutants displayed merely 14% and 30% ET of the wt activity (Table 5).

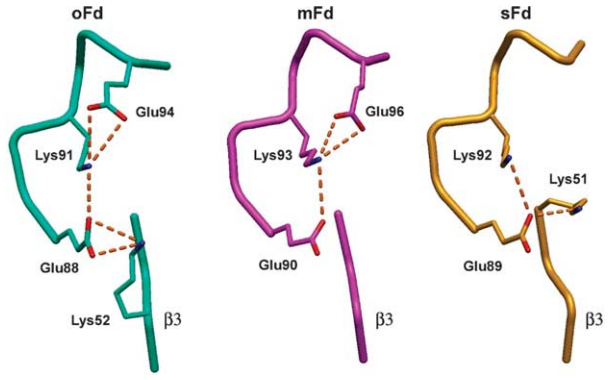

Figure 4. Network of salt bridges in different ferredoxin structures. The salt bridge network of ferredoxin from *S. oleracea*–(oFd; cyan), *M. laminosus*–(mFd; magenta), and *Synechocystis* sp. PCC 680–(sFd; gold) in the C terminus region, and a segment of β3 of the molecules. In oFd and mFd, the salt bridge networks around Lys91/93 are virtually identical. In sFd the salt bridge network is less complex, forming only two interactions around Glu89. In sFd the position equivalent to Glu94 and Glu96 of oFd and mFd, respectively, is replaced by an aspartate, which is too short to form salt bridge interactions.

Discussion

Previous studies have indicated that several factors may confer thermostable properties to a protein, often in concert.[12,14] This is supported by the factors found to confer thermostability to mFd in this study. Structural analysis of mFd revealed that its overall fold is similar to other plant-type mesophilic Fd structures. No significant differences were identified in the total number of hydrogen bond interactions or the packing density between mFd and four selected highly homologous structures of mesophilic Fds (Table 3). The most notable difference between mFd and the similar mesophilic homologues, aFd and pFd, is the presence of a salt bridge network in the C-terminal region of mFd (Figures 3 and 4; Table 4). A high number of salt bridge interactions is proposed to be one of the crucial factors that determine thermostability in proteins.[30,31] Furthermore, salt bridge networks are known to be energetically more favorable than an equivalent number of individual salt bridge interactions.[13,32] We thus conclude that the thermostability of mFd results, in part, from its salt bridge network at the C-terminal region. Conversely, aFd and pFd lack such a salt bridge network (Table 4) and although sFd and oFd exhibit a similar salt bridge network in their C-terminal region as mFd, they are mesophilic (Figure 4 and Table 6). This shows that additional molecular factor(s), other than salt bridge networks, must account for differences in the thermostability between mFd and the mesophilic sFd and oFd. The primary and tertiary structures of mFd, sFd, and oFd (Figure 3) revealed notable differences in the L1,2 loop region. In mFd, the L1,2 loop is located above the inner core of the protein, which is highly hydrophobic (Figure 2). The difference in the conformations of the L1,2 region in mFd, aFd and pFd, despite the high sequence identity in this region (Figure 3(a) and (b)), indicate that indeed this loop displays a substantial degree of flexibility and could increase the accessibility of the core to solvent. This

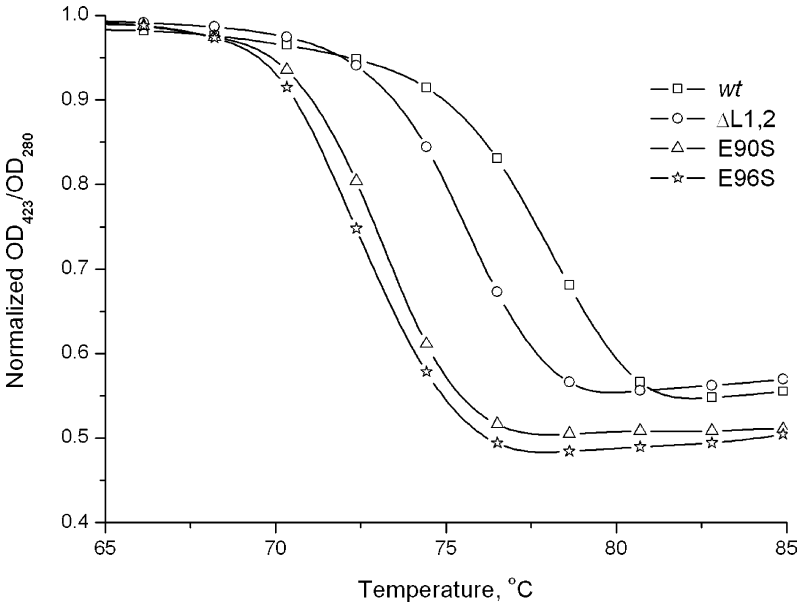

Figure 5. The thermal stability of the [2Fe-2S] cluster of mFd. Spectroscopic measurement of *M. laminosus* mFd and its three mutants (ΔL1,2, E90S, E96S) were measured in order to follow proper assembly of the their [2Fe-2S] clusters. The absorption at 280 nm and 423 nm was measured during continuous heating (1 deg. C/minute) of 200 μl samples containing wild-type (wt) *M. laminosus* ferredoxin (squares) and three of its mutants: ΔL1,2 (circles), E90S (triangles) and E96S (stars) at 50 μM. The drop in the ratio of 423 nm to 280 nm absorptions indicates the dissociation of the [2Fe-2S] cluster.

assumption is further supported by the disorder of L1,2 in molecule A of mFd. The sFd and oFd structures differ from mFd in the size and conformation of the L1,2 loop. In sFd and oFd L1,2 is two residues shorter than in mFd, aFd and pFd (Figure 3), and forms a rigid β-turn which blocks solvent access to the hydrophobic core of the protein. The increase of the hydrophobic ASA of a protein is a well-recognized thermostability determining factor.[33–35] It is possible that the flexibility in the L1,2 region alters the ASA in mFd due to increased motion at higher temperatures which exposes its hydrophobic core. This may contribute to the thermostable properties of the protein relative to sFd and oFd, which contain a rigid β-turn. The concept that shorter or more rigid loops increase protein thermostability[36,37] is not reflected in the case of mFd (Tables 3 and 6).

In order to analyze the individual factors that render mFd thermostable, three mutations were designed (ΔL1,2, E90S, and E96S). The thermostability of these mutants vis-à-vis the wt mFd, was assayed by monitoring the irreversible dissociation of the [2Fe-2S] cluster as a function of increased temperature (Figure 5). In addition, the ET activities of the mutated mFds were compared to that of the wt mFd (Table 5). The [2Fe-2S] cluster was less stable as a function of temperature in all three mutants in comparison to wt mFd (Figure 5). In the E90S and E96S mutants, the salt bridge networks near the C-terminal region are probably, at least, partially disrupted (Figure 4) and are in closer proximity to the [2Fe-2S] cluster in comparison to the distal L1,2 loop region. Indeed, these two mutants displayed similar [2Fe-2S] dissociation properties at temperatures approximately 10 deg. C lower than the cluster in the wt mFd (Figure 5). The loop replacement by a β-turn (ΔL1,2), however, caused a smaller (∼5 deg. C) decrease in the thermal stability of its cluster relative to the wt protein (Figure 5). ET activities of the three mutants indicate that the E96S mutant exhibits higher PSI photo-oxidation activity at 55 °C than the E90S mutant. To a large extent, these reduced ET activities were expected in both mutants with regard to the dissociation of the [2Fe-2S] clusters at higher temperatures (Figure 5). Conversely, the result indicating that ΔL1,2 did not have

Table 5. Photo-oxidation rate of photosystem I primary donor–P_{700} ($\Delta A_{820\ nm}$/s) by wt and mutants of mFd as a function of temperature

Temperature (°C)	mFd proteins			
	wt	ΔL1,2	E90S	E96S
23	53.3±7.0	48.9±5.0	39.8±5.6	44.7±5.7
55	72.7±17.7	4.5±8.3	10.4±8.6	22.5±9.3

The initial rate of the light-induced oxidation of photosystem I isolated from *M. laminosus*[47] in the presence of wild-type *M. laminosus* ferredoxin, or its mutants, was measured using the PAM-101 system.[29] The data are expressed in relative units s^{-1}, after subtracting the initial light-induced oxidation rate of photosystem I at each temperature in the absence of ferredoxin.

Table 6. Analyzed structural elements affecting protein thermostability

Molecule	C-terminal salt bridge network	Flexibility of L1,2
mFd	+	+
aFd	−	+
pFd	−	+
sFd	+	−
oFd	+	−

The structure featuring the property is indicated by (+), otherwise indicated by (−). Data are shown for molecule B of *M. laminosus* ferredoxin (mFd), *Anabaena* sp. PCC 7119 ferredoxin–(aFd),[26] *S. platensis* ferredoxin–(pFd),[24] *Synechocystis* sp. PCC 6803 ferredoxin–(sFd)[27] and *S. oleracea* ferredoxin–(oFd).[28]

ET activity at high temperatures was astonishing (Table 5): the thermal stability of the [2Fe-2S] cluster was higher relative to that of E90S and E96S, probably due to the distance of the L1,2 loop from the cluster. Surprisingly, the initial PSI photo-oxidation rate of ΔL1,2 was dramatically smaller at 55 °C in the ET assay (Table 5). These findings indicate that the E90S, E96S, and ΔL1,2 mutants behave differently with respect to their [2Fe-2S] stability and ET activities. This discrepancy may be attributed to differences in the association of the mutants with PSI. During photo-oxidation, the mFd binds PSI, accepts electrons and then dissociates from it. PSI binding may be involved in conformational changes of mFd that permit correct association and subsequent electron transfer. One may assume that at elevated temperatures the rigidity of the L1,2 β-turn of the ΔL1,2 mutant does not permit the conformational changes required for optimal association. This is despite the fact that at high temperatures (55 °C) the [2Fe-2S] cluster of ΔL1,2 displays higher stability than the clusters in the E90S, and E96S mutations, making it more capable of functioning in ET. These findings provide new insights into the interactions between PSI and Fd. In recent years, large efforts have been directed towards understanding the dynamics and interactions of Fd and the PSI reducing site subunits.[7] Analysis of the amino acids in Fd indicated the residues at the C terminus region of the Fd in the cluster of acidic residues (amino acid residues 92–95) as significant for PSI binding.[38] Here, for the first time, we show the involvement of mFd N-terminal amino acid residues (10–14).

In summary, structural analysis combined with functional assays presented here have provided two major innovative findings: the molecular factors that confer thermostability to mFd and new insights into the interactions of Fd with its electron donor, PSI. The results indicate that a combination of two factors, the salt bridge network and the flexibility of the L1,2 loop, render mFd thermostable where each factor taken individually is not sufficient to confer thermostability (Table 6). As in many other systems mFd thermostability is determined by a combination of small, subtle changes that are specific to the individual protein.[12–14,39,40] The finding that L1,2, which is distal from the [2Fe-2S] cluster, participates in the ET indicates cross-talk within the polypeptide chain that affects its activity.[41]

Materials and Methods

Crystallization, data collection, structure determination and refinement of mFd

mFd was isolated from *M. laminosus* cells, purified and crystallized by the vapor-diffusion, hanging-drop method as reported.[42] The mFd crystals belong to the orthorhombic space group $P2_12_12_1$ with cell parameters $a=28.5$ Å, $b=53.5$ Å, $c=111.7$ Å with two mFd molecules in the asymmetric unit.[42] Diffraction data to the resolution of 1.25 Å were collected at 100 K on a ADSC Quantum 4R CCD detector with an oscillation range of 0.5° and radiation wavelength of 0.933 Å at the European Synchrotron Radiation Facility (ESRF), Grenoble, France (beam line ID14-1). Data were integrated and scaled using the HKL suite.[43]

The mFd structure was solved *via* molecular replacement methods, using AMoRe[44] implemented in the CCP4 suite[45] using PDB code 1J7C as the search model. The space group was determined and verified *via* molecular replacement translation search. The structure was refined initially using the rigid body refinement procedure in CNS[21] at the resolution range of 20 Å–4.0 Å and was further refined using SHELX-97.[22] At each step the model was checked and fitted manually into the electron density maps using the graphic program O.[23]

mFd mutant cDNA constructs

All mFd mutants were prepared using standard PCR mutagenesis methods based on the wild-type mFd gene, cloned in pET20b (Novagen) ferredoxin. The E96S mutant was prepared by two oligonucleotide primers; the forward primer GGAGATATACATATGGCAACCTA TAAA containing the NdeI restriction site and the reverse primer GGTGGTGCTCGAGCTAGTAAAGCGATTCTTC containing the E96S mutation followed by the XhoI restriction site. The primers were used to amplify the E96S mutated gene that was subsequently cloned into the NdeI and XhoI sites in the pET20b vector. The ΔL1,2 replacement was done in a similar way, where the forward primer CATAGTTAAGCCAGTATACACTCC contained an AccI restriction site, and the reverse primer CTTCAATTGTTTTGTTACCTGTAGGGTTAATAAGTG TAACTTTATAGGTTCC contained the ΔL1,2 mutation and MfeI restriction site. The primers were used to amplify the ΔL1,2 mutated gene that was restricted and sub-cloned into the pET20b ferredoxin between the AccI and MfeI restriction sites in the gene.

The E90S mutant was prepared according to the PCR overlap extension method[46] using two internal primers; the internal forward CGTCATCTCAACACACAAA GAAGAAGAGCTTTAC and the internal reverse CTTCTTCTTTGTGTGTTGAGATGACGCAATC, both containing the E90S mutation region, and two external primers, the forward primer from the E90S mutant, containing the NdeI restriction site, and a reverse primer GCCCACTACGTGACCCATCACC containing the BanII site. After producing the fused mutated gene, the PCR product was cloned back into the pET20b ferredoxin construct using NdeI and BanII restriction sites, replacing the region between the pET20b ferredoxin construct. All oligonucleotide primers were obtained from MWG Biotech. All mutants were verified by DNA sequencing and were expressed and purified using the protocol described in our previous work.[42] Molecular masses of the three mFd mutants were verified by mass spectroscopic measurements.

Measurements of the thermal stability of the mFd [2Fe-2S] cluster and ET from PSI

The thermal stability of the [2Fe-2S] cluster of the wt and mutated mFds was determined by UV–VIS spectroscopic measurements. The characteristic absorbance of [2Fe-2S] at 423 nm was normalized to the absorbance of the protein moiety measured at 280 nm. Absorption measurements at wavelengths of 280 nm and 423 nm

were performed on a Cary 300 spectrophotometer (Varian Inc.). The measurements were conducted with continuous incremental heating of 1 deg. C/minute. Each sample contained a concentration of 50 μM protein in a volume of 200 μl.

The mFds ET activities were determined by measuring the initial photo-oxidation rate of PSI. The assay of PSI photo-oxidation was conducted by measuring the light induced absorption changes of the PSI primary donor, $P_{700,}$ at $A_{820\ nm}$. The measurements were performed with the PSI attachment of the Pulse Amplitude Modulated fluorimeter (PAM-101, Walz, Germany).[29] The 0.4 ml samples of 0.2 μM PSI from *M. laminosus*,[47] 10 μM mFd and 10 mM ascorbic acid in solution, containing 10 mM Tricine–HCl buffer (pH 8.0), 5 mM $MgCl_2$ and 0.03% *n*-dodecyl-β-D-maltoside, were exposed to saturating light (5000 μmol photons $m^{-2}\,s^{-1}$) for a duration of three seconds at different temperatures and the initial rate (absorbance changes in relative units)/second were calculated.

Acknowledgements

This work has been supported, in part, by the Israeli Science Foundation. We thank Dr D. E. Shalev from the NMR facility, and Dr M. Lebendiker from the Protein Purification Division of the Wolfson Centre for Applied Structural Biology for their advice and support, and the ESRF staff for their assistance during data collection. We thank Dr L. Shimon and Mrs M. Berman for their suggestions and assistance.

References

1. Holm, R. H., Kennepohl, P. & Solomon, E. I. (1996). Structural and functional aspects of metal sites in biology. *Chem. Rev.* **96**, 2239–2314.
2. Beinert, H., Holm, R. H. & Munck, E. (1997). Iron-sulfur clusters: nature's modular, multipurpose structures. *Science*, **277**, 653–659.
3. Johnson, M. K. (1998). Iron-sulfur proteins: new roles for old clusters. *Curr. Opin. Chem. Biol.* **2**, 173–181.
4. Knaff, D. B. & Hirasawa, M. (1991). Ferredoxin-dependent chloroplast enzymes. *Biochim. Biophys. Acta*, **1056**, 93–125.
5. Holden, H. M., Jacobson, B. L., Hurley, J. K., Tollin, G., Oh, B. H., Skjeldal, L. *et al*. (1994). Structure-function studies of [2Fe-2S] ferredoxins. *J. Bioenerg. Biomembr.* **26**, 67–88.
6. Cammack, R., Rao, K. K., Bargeron, C. P., Hutson, K. G., Andrew, P. W. & Rogers, L. J. (1977). Midpoint redox potentials of plant and algal ferredoxins. *Biochem. J.* **168**, 205–209.
7. Setif, P., Fischer, N., Lagoutte, B., Bottin, H. & Rochaix, J. D. (2002). The ferredoxin docking site of photosystem I. *Biochim. Biophys. Acta*, **1555**, 204–209.
8. Hase, T., Wakabayashi, S., Matsubara, H., Rao, K. K., Hall, D. O., Widmer, H. *et al*. (1978). The amino acid sequence of ferredoxin from the alga Mastigocladus laminosus. *Phytochemistry*, **17**, 1863–1867.
9. Matthews, B. W., Weaver, L. H. & Kester, W. R. (1974). The conformation of thermolysin. *J. Biol. Chem.* **249**, 8030–8044.
10. Perutz, M. F. & Raidt, H. (1975). Stereochemical basis of heat stability in bacterial ferredoxins and in haemoglobin A2. *Nature*, **255**, 256–259.
11. Zuber, H. (1988). Temperature adaptation of lactate dehydrogenase. Structural, functional and genetic aspects. *Biophys. Chem.* **29**, 171–179.
12. Scandurra, R., Consalvi, V., Chiaraluce, R., Politi, L. & Engel, P. C. (1998). Protein thermostability in extremophiles. *Biochimie*, **80**, 933–941.
13. Criswell, A. R., Bae, E., Stec, B., Konisky, J. & Phillips, G. N., Jr (2003). Structures of thermophilic and mesophilic adenylate kinases from the genus *Methanococcus*. *J. Mol. Biol.* **330**, 1087–1099.
14. Kumar, S. & Nussinov, R. (2001). How do thermophilic proteins deal with heat? *Cell. Mol. Life Sci.* **58**, 1216–1233.
15. Vieille, C. & Zeikus, G. J. (2001). Hyperthermophilic enzymes: sources, uses, and molecular mechanisms for thermostability. *Microbiol. Mol. Biol. Rev.* **65**, 1–43.
16. Kumar, S. & Nussinov, R. (1999). Salt bridge stability in monomeric proteins. *J. Mol. Biol.* **293**, 1241–1255.
17. Berman, H. M., Battistuz, T., Bhat, T. N., Bluhm, W. F., Bourne, P. E., Burkhardt, K. *et al*. (2002). The Protein Data Bank. *Acta Crystallog. sect. D*, **58**, 899–907.
18. Baumann, B., Sticht, H., Scharpf, M., Sutter, M., Haehnel, W. & Rosch, P. (1996). Structure of *Synechococcus elongatus* [Fe2S2] ferredoxin in solution. *Biochemistry*, **35**, 12831–12841.
19. Hatanaka, H., Tanimura, R., Katoh, S. & Inagaki, F. (1997). Solution structure of ferredoxin from the thermophilic cyanobacterium *Synechococcus elongatus* and its thermostability. *J. Mol. Biol.* **268**, 922–933.
20. Hurley, J. K., Weber-Main, A. M., Stankovich, M. T., Benning, M. M., Thoden, J. B., Vanhooke, J. L. *et al*. (1997). Structure–function relationships in Anabaena ferredoxin: correlations between X-ray crystal structures, reduction potentials, and rate constants of electron transfer to ferredoxin:NADP+ reductase for site-specific ferredoxin mutants. *Biochemistry*, **36**, 11100–11117.
21. Brunger, A. T., Adams, P. D., Clore, G. M., DeLano, W. L., Gros, P., Grosse-Kunstleve, R. W. *et al*. (1998). Crystallography & NMR system: a new software suite for macromolecular structure determination. *Acta Crystallog. sect D*, **54**, 905–921.
22. Sheldrick, G. M. & Schneider, T. (1997). High resolution refinement methods in enzymology. *Methods Enzymol.* **277**, 319–343.
23. Jones, T. A., Zou, J. Y., Cowan, S. W. & Kjeldgaard, M. (1991). Improved methods for building protein models in electron density maps and the location of errors in these models. *Acta Crystallog. sect. A*, **47**, 110–119.
24. Fukuyama, K., Ueki, N., Nakamura, H., Tsukihara, T. & Matsubara, H. (1995). Tertiary structure of [2Fe-2S] ferredoxin from *Spirulina platensis* refined at 2.5 Å resolution: structural comparisons of plant-type ferredoxins and an electrostatic potential analysis. *J. Biochem. (Tokyo)*, **117**, 1017–1023.
25. Orengo, C. A., Michie, A. D., Jones, S., Jones, D. T., Swindells, M. B. & Thornton, J. M. (1997). CATH–a hierarchic classification of protein domain structures. *Structure*, **5**, 1093–1108.
26. Morales, R., Charon, M. H., Hudry-Clergeon, G., Petillot, Y., Norager, S., Medina, M. & Frey, M. (1999). Refined X-ray structures of the oxidized, at 1.3 Å, and reduced, at 1.17 Å, [2Fe-2S] ferredoxin from the cyanobacterium Anabaena PCC7119 show redox-linked conformational changes. *Biochemistry*, **38**, 15764–15773.

27. van den Heuvel, R. H., Svergun, D. I., Petoukhov, M. V., Coda, A., Curti, B., Ravasio, S. *et al*. (2003). The active conformation of glutamate synthase and its binding to ferredoxin. *J. Mol. Biol.* **330**, 113–128.
28. Binda, C., Coda, A., Aliverti, A., Zanetti, G. & Mattevi, A. (1998). Structure of the mutant E92K of [2Fe-2S] ferredoxin I from Spinacia oleracea at 1.7 Å resolution. *Acta Crystallog. sect. D*, **54**, 1353–1358.
29. Klughammer, C. & Schreiber, U. (1994). An improved method, using saturating light pulses for the determination of photosystem I quantum yield *via* P700+, absorbance changes at 830 nm. *Planta*, **192**, 261–268.
30. Bogin, O., Levin, I., Hacham, Y., Tel-Or, S., Peretz, M., Frolow, F. & Burstein, Y. (2002). Structural basis for the enhanced thermal stability of alcohol dehydrogenase mutants from the mesophilic bacterium *Clostridium beijerinckii*: contribution of salt bridging. *Protein Sci.* **11**, 2561–2574.
31. Knochel, T., Pappenberger, A., Jansonius, J. N. & Kirschner, K. (2002). The crystal structure of indole-glycerol-phosphate synthase from *Thermotoga maritima*. Kinetic stabilization by salt bridges. *J. Biol. Chem.* **277**, 8626–8634.
32. Yip, K. S., Stillman, T. J., Britton, K. L., Artymiuk, P. J., Baker, P. J., Sedelnikova, S. E. *et al*. (1995). The structure of *Pyrococcus furiosus* glutamate dehydrogenase reveals a key role for ion-pair networks in maintaining enzyme stability at extreme temperatures. *Structure*, **3**, 1147–1158.
33. Auerbach, G., Ostendorp, R., Prade, L., Korndorfer, I., Dams, T., Huber, R. & Jaenicke, R. (1998). Lactate dehydrogenase from the hyperthermophilic bacterium thermotoga maritima: the crystal structure at 2.1 Å resolution reveals strategies for intrinsic protein stabilization. *Structure*, **6**, 769–781.
34. Hashimoto, H., Inoue, T., Nishioka, M., Fujiwara, S., Takagi, M., Imanaka, T. & Kai, Y. (1999). Hyperthermostable protein structure maintained by intra and inter-helix ion-pairs in archaeal O6-methylguanine-DNA methyltransferase. *J. Mol. Biol.* **292**, 707–716.
35. Machius, M., Declerck, N., Huber, R. & Wiegand, G. (2003). Kinetic stabilization of *Bacillus licheniformis* alpha-amylase through introduction of hydrophobic residues at the surface. *J. Biol. Chem.* **278**, 11546–11553.
36. Russell, R. J., Ferguson, J. M., Hough, D. W., Danson, M. J. & Taylor, G. L. (1997). The crystal structure of citrate synthase from the hyperthermophilic archaeon pyrococcus furiosus at 1.9 Å resolution. *Biochemistry*, **36**, 9983–9994.
37. Thompson, M. J. & Eisenberg, D. (1999). Transproteomic evidence of a loop-deletion mechanism for enhancing protein thermostability. *J. Mol. Biol.* **290**, 595–604.
38. Floss, B., Igloi, E. G., Cassier-Chauvat, C. & Muhlenhoff, U. (1997). Molecular characterization and overexpression of the petF gene from *Synechococcus elongatus*: evidence for a second site of electrostatic interaction between ferredoxin and the PS I-D subunit. *Photosynth. Res.* **54**, 63–71.
39. Jaenicke, R. & Bohm, G. (1998). The stability of proteins in extreme environments. *Curr. Opin. Struct. Biol.* **8**, 738–748.
40. Demirjian, D. C., Moris-Varas, F. & Cassidy, C. S. (2001). Enzymes from extremophiles. *Curr. Opin. Chem. Biol.* **5**, 144–151.
41. Covalt, J. C., Jr, Roy, M. & Jennings, P. A. (2001). Core and surface mutations affect folding kinetics, stability and cooperativity in IL-1 beta: does alteration in buried water play a role? *J. Mol. Biol.* **307**, 657–669.
42. Fish, A., Lebendiker, M., Nechushtai, R. & Livnah, O. (2003). Purification, crystallization and preliminary X-ray analysis of ferredoxin isolated from thermophilic cyanobacterium *Mastigocladus laminosus*. *Acta Crystallog. sect. D*, **59**, 734–736.
43. Otwinowski, Z. & Minor, W. (1997). Processing X-ray data collected in oscillation mode. *Methods Enzymol.* **276**, 307–325.
44. Navaza, J. (2001). Implementation of molecular replacement in AMoRe. *Acta Crystallog. sect. D*, **57**, 1367–1372.
45. Collaborative Computing Project, Number 4 (1994). The CCP4 suite: programs for protein crystallography. *Acta Crystallog. sect. D*, **50**, 760–763
46. Senanayake, S. D. & Brian, D. A. (1995). Precise large deletions by the PCR-based overlap extension method. *Mol. Biotechnol.* **4**, 13–15.
47. Almog, O., Shoham, G., Michaeli, D. & Nechushtai, R. (1991). Monomeric and trimeric forms of photosystem I reaction center of *Mastigocladus laminosus*: crystallization and preliminary characterization. *Proc. Natl Acad. Sci. USA*, **88**, 5312–5316.
48. Esnouf, R. M. (1999). Further additions to MolScript version 1.4, including reading and contouring of electron-density maps. *Acta Crystallog. sect. D*, **55**, 938–940.
49. Kraulis, P. J. (1991). MOLSCRIPT: a program to produce both detailed and schematic plots of protein structures. *J. Appl. Crystallog.* **24**, 946–950.
50. Ferrin, T. E., Huang, C. C., Jarvis, L. E. & Langridge, R. (1988). The MIDAS display system. *J. Mol. Graph.* **6**, 13–27.
51. Thompson, J. D., Higgins, D. G. & Gibson, T. J. (1994). CLUSTAL W: improving the sensitivity of progressive multiple sequence alignment through sequence weighting, position-specific gap penalties and weight matrix choice. *Nucl. Acids Res.* **22**, 4673–4680.
52. Laskowski, R. A., MacArthur, M. W., Moss, D. S. & Thornton, J. M. (1993). PROCHECK: a program to check the sterochemical quality of protein structures. *J. Appl. Crystallog.* **26**, 283–291.
53. McDonald, I. K. & Thornton, J. M. (1994). Satisfying hydrogen bonding potential in proteins. *J. Mol. Biol.* **238**, 777–793.
54. Nicholls, A., Sharp, K. A. & Honig, B. (1991). Protein folding and association: insights from the interfacial and thermodynamic properties of hydrocarbons. *Proteins: Struct. Funct. Genet.* **11**, 281–296.
55. Barlow, D. J. & Thornton, J. M. (1983). Ion-pairs in proteins. *J. Mol. Biol.* **168**, 867–885.

Edited by M. Guss

(Received 8 March 2005; received in revised form 26 April 2005; accepted 28 April 2005)